

Article

Sensitivity Analysis of Influencing Factors of Underground Civil Air Defense Construction Vibration under Vehicle Load

Yangyong Wu ^{1,2} , Chaomin Mu ^{1,2,*}, Hui Zhang ² and Hui Zhou ¹

¹ State Key Laboratory of Mining Response and Disaster Prevention and Control in Deep Coal Mines, Huainan 232001, China

² School of Safety Science and Engineering, Anhui University of Science and Technology, Huainan 232001, China

* Correspondence: chmmu@mail.ustc.edu.cn

Abstract: Abstract Grey correlation theory is an uncertainty analysis method, which can find the relevance of various factors studied through certain data processing in incomplete information and find the main influencing factors. In order to study the influence of vehicle load on the vibration of underground civil air defense construction, taking the civil air defense construction at the intersection of Zhongzhou Middle Road and Shachang South Road in Luoyang as the study subject, based on the field measured data, and using ANSYS to expand the working conditions, this paper studies the influence of such factors as elastic modulus of concrete, thickness of overburden layer, density of soil layer, elastic modulus of soil layer, vehicle speed, and vehicle mass on the vibration of the civil air defense construction through the grey correlation sensitivity analysis method. The field measurement and numerical simulation results show that the displacement, velocity, and acceleration values decrease gradually from the mid-span position of the roof to the wall. Displacement, velocity, and acceleration are important indexes for evaluating vibration. The grey correlation degree of the influencing factors of displacement and velocity from large to small is density of soil layer, vehicle mass, vehicle speed, elastic modulus of concrete, elastic modulus of soil layer, and thickness of overburden layer. The grey correlation degree of the influencing factors of acceleration from large to small is vehicle mass, layer of density of soil layer, vehicle speed, elastic modulus of concrete, elastic modulus of soil layer, and thickness of overburden layer. The grey correlation degree of soil layer density, vehicle mass and vehicle speed to displacement, velocity, and acceleration is 0.7951–0.9993, which indicates that their influence is significant. This study can provide reference for the design and construction of similar civil air defense constructions.

Keywords: vehicle load; civil air defense constructions; grey correlation degree; sensitivity analysis; vibration



Citation: Wu, Y.; Mu, C.; Zhang, H.; Zhou, H. Sensitivity Analysis of Influencing Factors of Underground Civil Air Defense Construction Vibration under Vehicle Load. *Appl. Sci.* **2022**, *12*, 12361. <https://doi.org/10.3390/app122312361>

Academic Editor: Junhong Park

Received: 4 November 2022

Accepted: 1 December 2022

Published: 2 December 2022

Publisher's Note: MDPI stays neutral with regard to jurisdictional claims in published maps and institutional affiliations.



Copyright: © 2022 by the authors. Licensee MDPI, Basel, Switzerland. This article is an open access article distributed under the terms and conditions of the Creative Commons Attribution (CC BY) license (<https://creativecommons.org/licenses/by/4.0/>).

1. Introduction

With the continuous expansion of the city size and the continuous increase in urban population, it is difficult to meet the growing demand for life on the limited ground space. Therefore, in order to expand the living space of citizens, it is necessary to develop and utilize urban underground space, such as building subways, underground commercial streets, and civil air defense constructions [1–3]. The shallow-buried underground excavation method is often used to build underground civil air defense constructions and subways in cities [4–6]. The underground commercial street and underpass of the civil air defense constructions are located under the road or square in the downtown area of the city. Such constructions are generally close to the ground. Although the cut and cover method is economical, it affects the traffic of the road and the business of shops on both sides of the road [7–9]. In order to avoid this problem, it is a wise choice to adopt the shallow-buried excavation method for the construction of civil air defense. The most important thing for underground constructions is to prevent them from being affected by earthquake excitation [10,11]. Underground constructions are vulnerable to traffic vibration. Because

the thickness of the overburden layer of the roof of the underground civil air defense construction is relatively thin, the vibration generated by vehicles traveling on the road is transferred to the underground civil air defense construction, causing the civil air defense construction to vibrate, which has adverse effects on the shallow-buried and concealed excavation construction, such as the sand falling from the roof.

The existing research on vehicle load mainly focuses on the influence of vehicle load on settlement. Zou et al. [12] simulated the settlement of vehicle load on the soil mass in the reclamation area based on the finite element software ABAQUS, and obtained that the settlement curve generated by vehicle load is normally distributed; Zhang et al. [13] based on a river crossing tunnel of Wuhan Metro Line 2, studied the impact of train load on the rail settlement, and concluded that the rail settlement and train load are linear positive correlation; Li et al. [14] studied the settlement of soil around the road shield tunnel under random vehicle load based on the random dynamic vehicle load model, and obtained that the maximum settlement is about 1/10 of the subway tunnel; Li et al. [15] proposed a sequential probability back analysis method based on Bayesian subset, which can monitor and analyze the ground settlement of the tunnel in real time; Zhou et al. [16] studied the dynamic response law and long-term cumulative deformation of saturated soft clay foundation under subway train load based on consolidation undrained triaxial tests; Wang et al. [17] studied the cumulative settlement of the railway track transition zone based on the iterative procedure; Meng et al. [18] studied the dynamic deformation response law of subgrade through dynamic loading–unloading test of subgrade under vehicle load; Shi et al. [19] studied the influence of tunnel settlement on vibration of saturated porous elastic foundation based on Biot theory; Ma et al. [20] studied the dynamic response of vehicle load to remolded loess subgrade through tests.

The research on the structural vibration response caused by vehicle load only focuses on the dynamic response of the structure caused by vehicle driving vibration inside the structure. Shao et al. [21] used ANSYS software to simulate the vibration response of traffic load to the initial support of tunnel portal; Jia et al. [22] calculated the vibration response of the subway structure to the subway train through the load number determination method and analytical formula method; Galvin et al. [23] used the three-dimensional time-domain boundary element to represent soil, ballast, and structure, and proposed a general numerical model that can analyze soil movement caused by train running; Zhou et al. [24] proposed a vertical coupling model of train track tunnel soil, and studied the train dynamic response law; Hu et al. [25] studied the propagation law of dynamic response of train load in surrounding soil based on test and numerical simulation; Yan et al. [26] proposed a concrete constitutive model under uniaxial cyclic loading considering the fatigue damage of concrete, and studied the cumulative damage of tunnel crossing structures when trains are running; Yang et al. [27] studied the fatigue damage caused by the train to the three-dimensional cross tunnel in the long-term running process; Zhang et al. [28] considering the axle load and unsprung mass of the car body, studied the dynamic response law of the heavy haul train to the tunnel; Lai et al. [29] analyzed the vibration response law of subway train load to shield tunnel structure from the perspective of displacement, velocity, and acceleration based on three-dimensional dynamics. The dynamic response of underground structures to ground vehicle-induced vibration is rarely studied.

Grey correlation analysis was proposed by Professor Deng [30]. This method is used to find the factors that have the greatest impact on the target factors by calculating the main relationship between the target factors and the corresponding factors. By quantifying the relationship between them, it can quantitatively explain the interrelationship between the change factors and the corresponding factors [31]. Hu et al. [32] analyzed many factors affecting pavement damage based on grey correlation analysis method. Xie et al. [33] studied the impact of traffic flow, alignment, and sign information on drivers' behavior based on the gray correlation method. The grey correlation method is an uncertainty analysis method, which is very suitable for finding the main influencing factors in some uncertain factors.

According to the previous contents, previous studies mainly involved the influence of vehicle load on settlement and the vibration of the tunnel caused by vehicle load in the underground tunnel. The influence of ground vehicle load on the vibration of underground buildings is rarely studied, especially the influence of ground vehicle load on the vibration of underground civil air defense construction under construction. In order to study the impact of vehicle load on the vibration of underground civil air defense construction, this paper takes the civil air defense construction at the intersection of Zhongzhou Middle Road and Shachang South Road in Luoyang City as the study subject, based on the field measurement, the author uses the ANSYS numerical software to conduct a transient analysis, and studies the influence of vehicle load on the civil air defense construction vibration when the influence factors such as the elastic modulus of concrete, the thickness of overburden layer, the density of soil layer, the elastic modulus of soil layer, vehicle speed, and vehicle mass change through the sensitivity analysis method of grey correlation.

2. Grey Correlation Analysis

As a part of the grey system, grey correlation analysis finds out their correlation and main influencing factors by processing and analyzing various factors to be studied, which is particularly suitable for the analysis and evaluation of influencing factors of roof mid-span displacement, velocity, and acceleration of civil air defense construction. The flow chart of grey correlation analysis is shown in Figure 1. The specific calculation steps of this method are as follows:

1. List comparison data matrix and reference data matrix:

The n factors (elastic modulus of concrete, thickness of overburden layer, density of soil layer, elastic modulus of soil layer, vehicle speed, and vehicle mass) that affect the mid-span displacement, velocity, and acceleration of civil air defense construction are taken as comparison series X , $X = (X_1 X_2 \dots X_n)^T$, and the corresponding mid-span displacement, velocity, and acceleration of roof are taken as reference series Y , $Y = (Y_1 Y_2 \dots Y_n)^T$. Each factor of columns X and Y has several values:

$$X_i = (X_i(1) X_i(2) X_i(3) X_i(4)) \tag{1}$$

$$Y_i = (Y_i(1) Y_i(2) Y_i(3) Y_i(4)) \tag{2}$$

Columns X and Y are written in matrix form:

$$X = \begin{pmatrix} X_1 \\ X_2 \\ \vdots \\ X_n \end{pmatrix} = \begin{pmatrix} X_1(1) & X_1(2) & \dots & X_1(4) \\ X_2(1) & X_2(2) & \dots & X_2(4) \\ \vdots & \vdots & \dots & \vdots \\ X_n(1) & X_n(2) & \dots & X_n(4) \end{pmatrix} \tag{3}$$

$$Y = \begin{pmatrix} Y_1 \\ Y_2 \\ \vdots \\ Y_n \end{pmatrix} = \begin{pmatrix} Y_1(1) & Y_1(2) & \dots & Y_1(4) \\ Y_2(1) & Y_2(2) & \dots & Y_2(4) \\ \vdots & \vdots & \dots & \vdots \\ Y_n(1) & Y_n(2) & \dots & Y_n(4) \end{pmatrix} \tag{4}$$

2. Dimensionless treatment of matrix:

The dimensionless methods of data are divided into initial value, average value, interval relative value, and normalization methods. X and Y are dimensionless through interval relative value.

$$X'_i = (X'_i(1) X'_i(2) X'_i(3) X'_i(4)) \tag{5}$$

where

$$X'_i(j) = \frac{X_i(j) - \min_j X_i(j)}{\max_j X_i(j) - \min_j X_i(j)} \tag{6}$$

At the same time, the reference column Y_i is dimensionless.

- Solving the grey correlation discernibility information of matrix:

The discernibility matrix Δ is solved by the following formula:

$$\Delta_{ij} = |Y'_i(j) - X'_i(j)| \tag{7}$$

Select the maximum and minimum values in Δ :

$$\begin{cases} \Delta_{max} = \max(\Delta_{ij}) \\ \Delta_{min} = \min(\Delta_{ij}) \end{cases} \tag{8}$$

- Solving the grey correlation coefficient matrix and grey correlation degree:

The calculation equation of grey correlation coefficient is:

$$\gamma_{ij} = \frac{\Delta_{min} + \zeta\Delta_{max}}{\Delta_{ij} + \zeta\Delta_{max}} \tag{9}$$

where ζ is the resolution coefficient, $\zeta \in [0, 1]$, and generally $\zeta = 0.5$.

By calculating the average value of the grey correlation coefficient as the correlation degree, the problem of large and scattered grey correlation coefficients is solved. The calculation equation of the grey correlation degree is:

$$A_i = \frac{1}{m} \sum_{j=1}^m \gamma_{ij} \tag{10}$$

The value range of the grey correlation degree is $[0, 1]$. The ranking of the grey correlation degree value reflects the sensitivity of the influencing factors. The larger the grey correlation degree value, the stronger the correlation between the comparison factors and the reference factors.

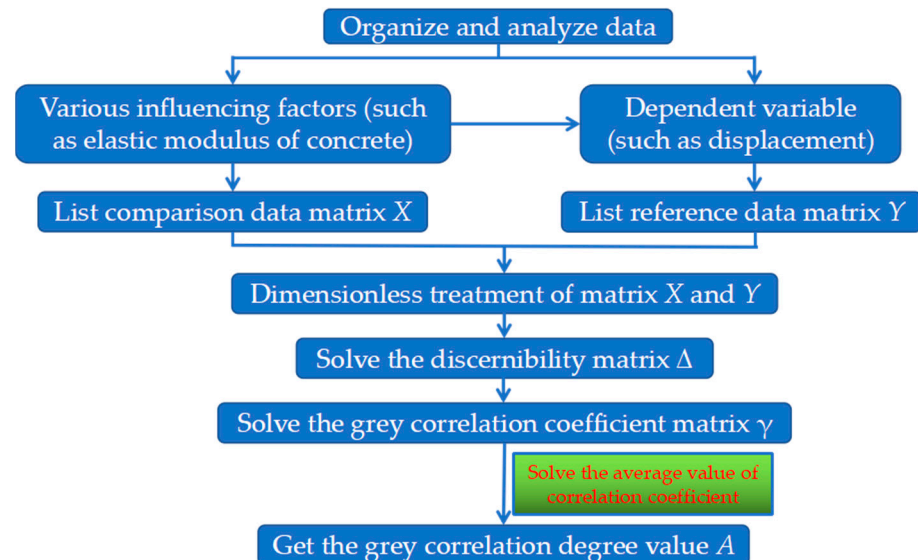


Figure 1. Flow chart of grey correlation analysis.

3. Field Measurement

This paper is based on the civil air defense construction introduced in references [34,35]. The civil air defense construction is located at the intersection of Zhongzhou Middle Road and Shachang South Road in Luoyang City.

3.1. Background Overview

The covering soil thickness of the main structure is 2.8 m, the span of the structure axis is 7.5 m, the surrounding business is prosperous, and the traffic on the road is busy. The dynamic load caused by frequent vehicle traffic has caused many adverse effects to the construction. The civil air defense construction needs to be monitored. The location of the construction is shown in Figure 2, and the ground road condition of the measuring point is shown in Figure 3. When the ground road passes normally, the acceleration of the underground civil air defense construction is monitored to study the vibration of the civil air defense construction under the condition of vehicle passing.



Figure 2. Schematic diagram of project location.

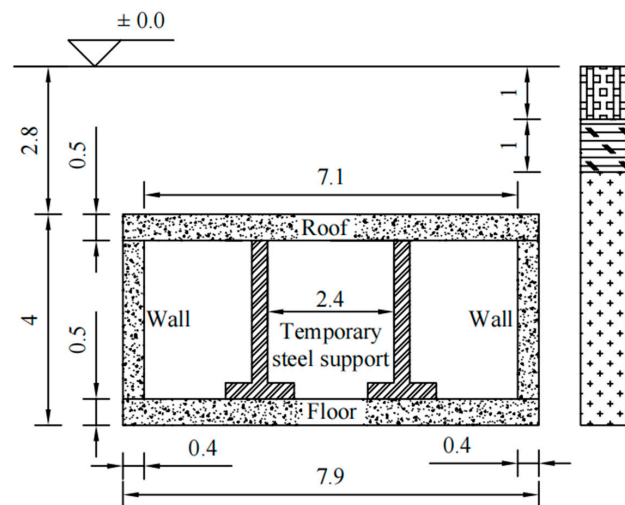


Figure 3. Schematic diagram of ground road above the measuring point [34].

3.2. Test Plan

Because the vibration response of each point of the structure is very different, it is very important to choose the appropriate installation location. In the construction process, since the soil in front of the working face has not been excavated yet but the rear of the working face has been supported, their bearing capacity is relatively good and the working face is the weakest, so the measuring points are arranged near the working face. Six measuring points are arranged along the horizontal direction on the constructed reinforced concrete roof near the working face to study and analyze the horizontal propagation law of vibration caused by road vehicles in the structure. The measuring points are arranged along the center of the road towards the sidewalk. The profile of the underground civil air defense

construction is shown in Figure 4. The distribution diagram of measuring points on the roof of the reinforced concrete structure is shown in Figure 5. An iron block should be pasted on each measuring point on the reinforced concrete surface with A/B glue in advance so as to fix the acceleration sensor during the test. The sensor should be a broadband acceleration sensor, and the sensitivity of the acceleration sensor should be greater than 100 mV/g. The gain of the amplification system should be greater than 60 dB, and the long-term variation should be less than 1%. The actual layout of the acceleration sensor is shown in Figure 6. The vibration of the structure mainly comes from road vehicles and nearby civil construction activities. The period 10:00–13:00 was chosen every day for measurement, which is the peak period of traffic flow. At the same time, it is the time for construction workers to have lunch and rest, which excludes the impact of civil construction activities.



Note: The unit in the figure is m.

Figure 4. The profile of the underground civil air defense construction [35].

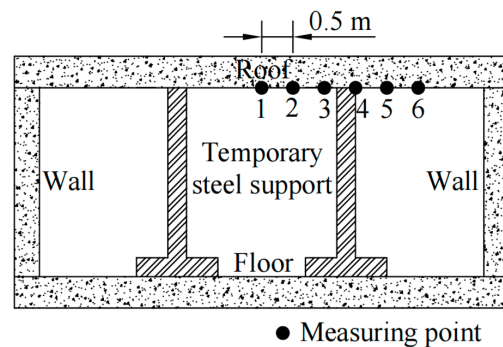


Figure 5. Schematic diagram of test point distribution [34].



Figure 6. Actual layout of the acceleration sensor [34].

3.3. Test Result

Model 6221 dynamic data acquisition instrument was used for the field test, dynamic data acquisition, and processing system as shown in Figure 7. The test system is composed of acceleration sensor, 6221 dynamic data acquisition instrument, and notebook computer. The test results are shown in Table 1. The acceleration is the average value of the test period in Table 1. The typical measured acceleration time–history curve (measuring point 1) of a certain period is intercepted as shown in Figure 8.

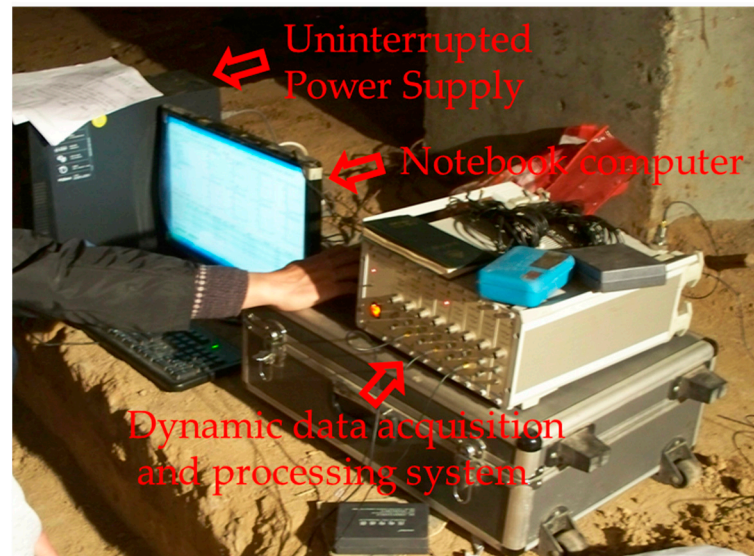


Figure 7. Dynamic data acquisition and processing system [34].

Table 1. Vibration test results [34].

Measuring Point	1	2	3	4	5	6
Acceleration ($\text{mm}\cdot\text{s}^{-2}$)	112	172	70	3	96	50

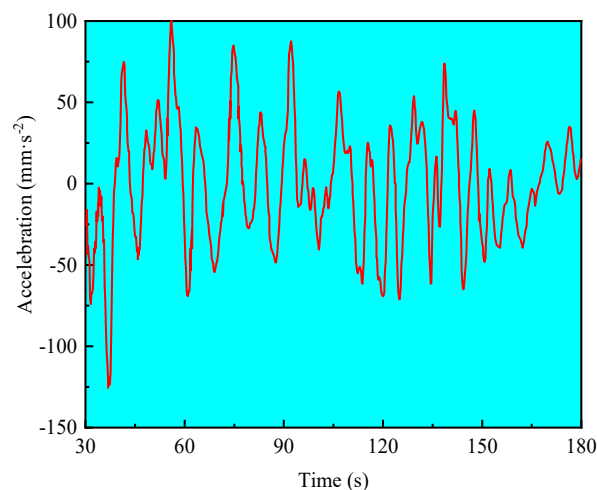


Figure 8. Typical measured acceleration time–history curve [34].

It can be seen from Table 1 and Figure 8 that the acceleration on the roof is generally $\pm 100 \text{ mm}\cdot\text{s}^{-2}$ to $\pm 200 \text{ mm}\cdot\text{s}^{-2}$, the vibration period is 3–6 s, and the frequency is 0.17–0.33 Hz. Although the acceleration value of the measuring point in the direction from the road center to the sidewalk does not strictly follow the law of becoming smaller and smaller, the acceleration value near the road center is obviously greater than that far away from the road center. The acceleration near the road center is $112\text{--}172 \text{ mm}\cdot\text{s}^{-2}$, and the

acceleration far from the road center is $50\text{--}96\text{ mm}\cdot\text{s}^{-2}$. Combined with the actual situation of the site construction, during the earthwork excavation during the peak hours of the day, there is sand falling from the top. However, if the excavation is conducted at night, the sand falling from the top is much less than that during the day, indicating that the impact of vibration caused by vehicle traffic on the earthwork excavation of civil air defense construction is relatively obvious. When the vibration acceleration is less than 100, the impact of vehicle traffic on excavation is small. Therefore, the earthwork excavation construction should avoid the rush hour of vehicles as much as possible. The tunnel excavation should be arranged at the time when the traffic flow is low at night. After the excavation, the initial support and shotcrete sealing should be carried out in time to prevent the damage of the formed tunnel caused by the vehicle vibration during the rush hour of vehicles in the daytime.

4. Numerical Simulation of the Influence of Vehicle Load on Civil Air Defense Construction Vibration

ANSYS software is used for numerical simulation calculation, based on the transient analysis, the law of vibration of underground civil air defense construction caused by vehicle load when the elastic modulus of concrete, thickness of overburden layer, density of soil layer, elastic modulus of soil layer, vehicle speed, and vehicle mass change is studied.

4.1. Model Introduction

According to the actual project, the calculation model is properly simplified to analyze the propagation law of driving vibration in civil air defense construction. The width of the calculation model is 20 m, the height is 13 m, and the axial length is 70 m. The soil layer is divided into three layers. The height of the first layer and the second layer is 1 m, and the height of the third layer is 11 m. The project section is shown in Figure 9. The supporting structure of civil air defense construction is reinforced concrete, with a covering thickness of 3 m, a height of 4 m, a width of 8 m, and a thickness of 0.5 m for the floor, roof and wall. SOLID45 solid element is selected for soil layer and civil air defense structure, which has many functions such as stress stiffening, expansion, creep, plasticity, large strain, large deformation, etc., so it can be used as an ideal element for simulating geotechnical materials. The numerical calculation model has 139,720 elements after meshing. The left and right boundaries are fixed with X direction displacement, the bottom boundary is fixed with Y direction displacement, and the front and rear boundaries are fixed with Z direction displacement. The components are connected by common nodes. The numerical simulation adopts transient analysis, and the time step is 0.03 s. The calculation model is shown in Figure 10.

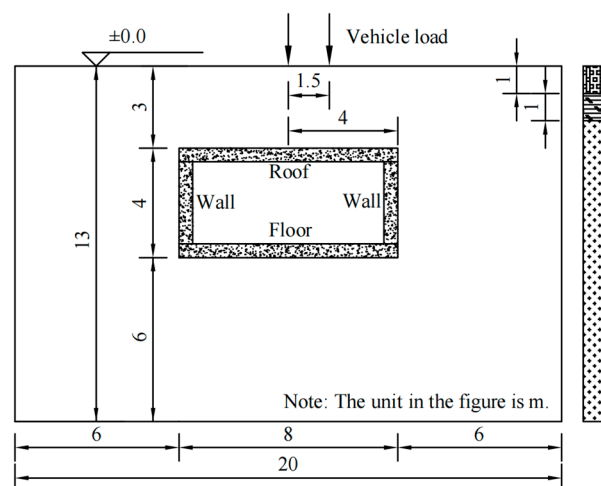


Figure 9. Project section.

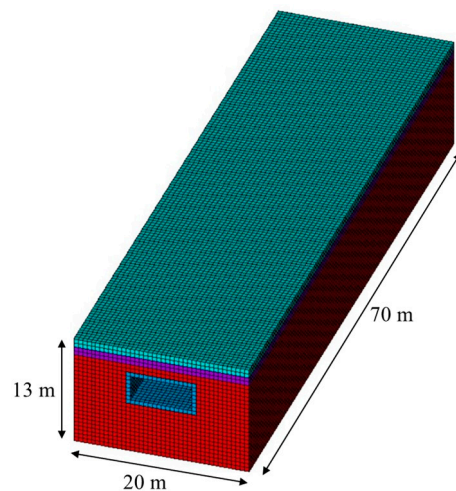


Figure 10. Numerical calculation model.

4.2. Numerical Simulation Conditions

The concrete density of the supporting structure of civil air defense works is $2500 \text{ kg}\cdot\text{m}^{-3}$, Poisson’s ratio is 0.2, and the Poisson’s ratio of the three layers of soil is 0.3. Other parameters and specific working conditions are shown in Table 2.

Table 2. Numerical simulation conditions.

Order Number	Elastic Modulus of Concrete (GPa)	Thickness of Overburden Layer (m)	Density of Soil Layer ($\text{kg}\cdot\text{m}^{-3}$)			Elastic Modulus of Soil Layer (MPa)			Vehicle Speed (km/h)	Vehicle Mass (kN)
			1st Layer	2nd Layer	3rd Layer	1st Layer	2nd Layer	3rd Layer		
1	32.5/34.5/36/37	3	1800	1850	1870	3	5	7	60	20
2	32.5	3/4/5/6	1800	1850	1870	3	5	7	60	20
3	32.5	3	1750/1800/1850/1900			3	5	7	60	20
4	32.5	3	1800			1/3/5/7			60	20
5	32.5	3	1800	1850	1870	3	5	7	15/30/45/60	20
6	32.5	3	1800	1850	1870	3	5	7	60	20/40/60/80

4.3. Vehicle Load

The load calculation example of a certain type of car is selected. The vehicle weight P_0 is 20 kN, the vehicle length L is 4 m, the distance between left and right tires is 1.5 m, the distance between front and rear tires is 2.0 m, and the vehicle speed v is 60 km/h. The vehicle load is simplified as a concentrated load. The vehicle load is simulated by using steady sine wave vibration. Considering the vehicle weight and speed, the vehicle load calculation expression is as follows [36]:

$$P = P_0 + P_d \tag{11}$$

where P_0 is the static load of the vehicle; P_d is the dynamic load of the vehicle.

$$P_d = M_0\alpha\omega^2\sin(\omega t) \tag{12}$$

where M_0 is the unsprung mass of the vehicle, and the value is $120 \text{ N}\cdot\text{s}^2/\text{m}$; α is the sagittal height, taken as 2 mm; $\omega = 2\pi v/L$.

The numerical value is substituted into the vehicle load expression as follows:

$$P = 20,000 + 164.49\sin(26.18t) \tag{13}$$

The load expression of a single tire is:

$$P' = 5000 + 41.12\sin(26.18t) \tag{14}$$

The vehicle load is applied at the mid-span of the civil air defense construction. The vehicle load is a concentrated load moving along the axial node and its value is sinusoidal, and it is evenly distributed at the four tires. The numerical calculation loading diagram is shown in Figure 11.

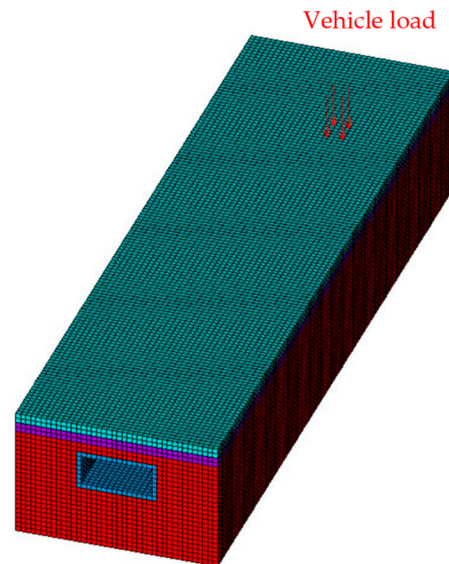


Figure 11. Schematic diagram of numerical calculation loading.

4.4. Layout of Measuring Points

Five measuring points are set along the bottom of the roof in the horizontal direction. The measuring points are arranged from the mid-span position to the wall direction. The spacing between adjacent measuring points is 1 m. The distribution diagram of measuring points is shown in Figure 12.

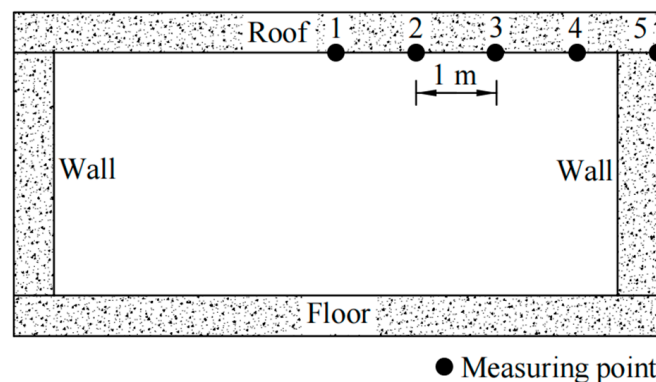


Figure 12. Schematic diagram of numerical simulation measuring point distribution.

5. Change Rule of Displacement, Velocity, and Acceleration

The typical time-history curve of displacement, velocity, and acceleration of the mid-span measuring point of the civil air defense construction is shown in Figure 13. At this time, the elastic modulus of concrete is 32.5 GPa. The change rule of displacement, velocity, and acceleration peak value of the measuring point in the horizontal split direction is shown in Figure 14. It can be seen from Figure 10 that the displacement, velocity, and acceleration at the mid-span position are maximum, and they are smaller and smaller along the top plate from the mid-span position to the wall.

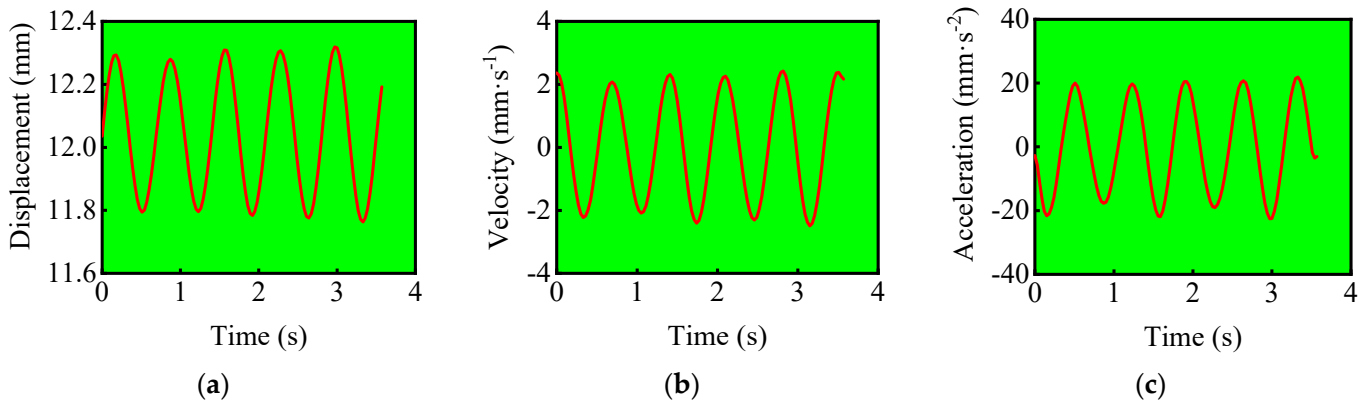


Figure 13. Typical time–history curve (a) displacement, (b) velocity, and (c) acceleration.

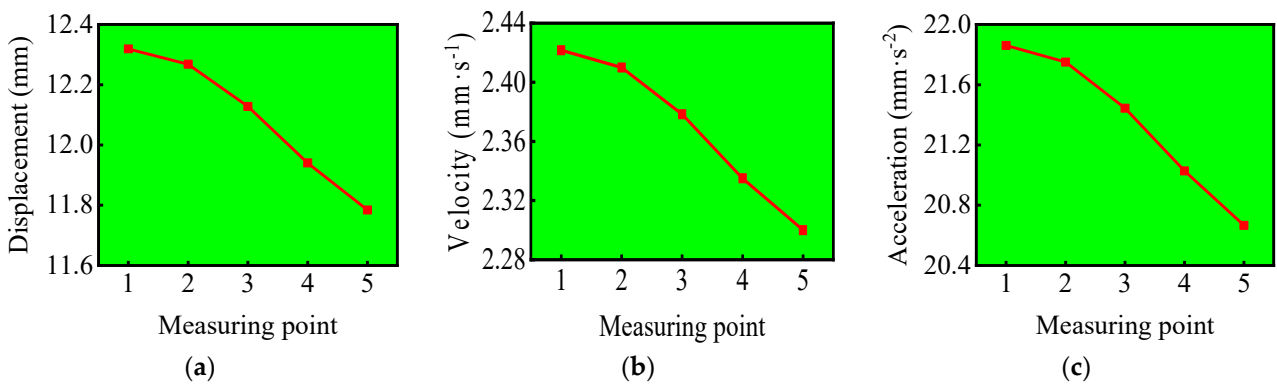


Figure 14. Peak value variation rule of measuring points under typical working condition (a) displacement, (b) velocity, and (c) acceleration.

5.1. Elastic Modulus of Concrete

When the elastic modulus of concrete changes, the change rules of displacement, velocity, and acceleration at different measuring points of civil air defense construction caused by vehicle vibration are shown in Figure 15. The results of displacement, velocity, and acceleration peak values at mid–span measuring points are shown in Table 3. The change rules of displacement, velocity, and acceleration peak values at mid–span measuring points are shown in Figure 16. When the elastic modulus of concrete is 32.5, 34.5, 36.0, and 37.0 GPa, the peak value of the mid–span displacement of the roof of the civil air defense construction is 12.3189, 12.2768, 12.2477, and 12.2293 mm, respectively, the peak value of velocity is 2.4217, 2.405, 2.395, and 2.3883 mm·s^{−1}, respectively, and the peak value of acceleration is 21.8611, 21.6667, 21.5833, and 21.5278 mm·s^{−2}, respectively. The results show that the peak value of displacement, velocity, and acceleration in the middle span of the roof decreases with the increase in the elastic modulus of concrete. With the increase in the elastic modulus of concrete by 6.15%, 10.77%, and 13.85%, the corresponding peak value of displacement in the middle span of the roof decreases by 0.34%, 0.58%, and 0.73%, respectively, the peak value of velocity decreases by 0.69%, 1.10% and 1.38%, respectively, and the peak value of acceleration decreases by 0.89%, 1.27% and 1.52%, respectively.

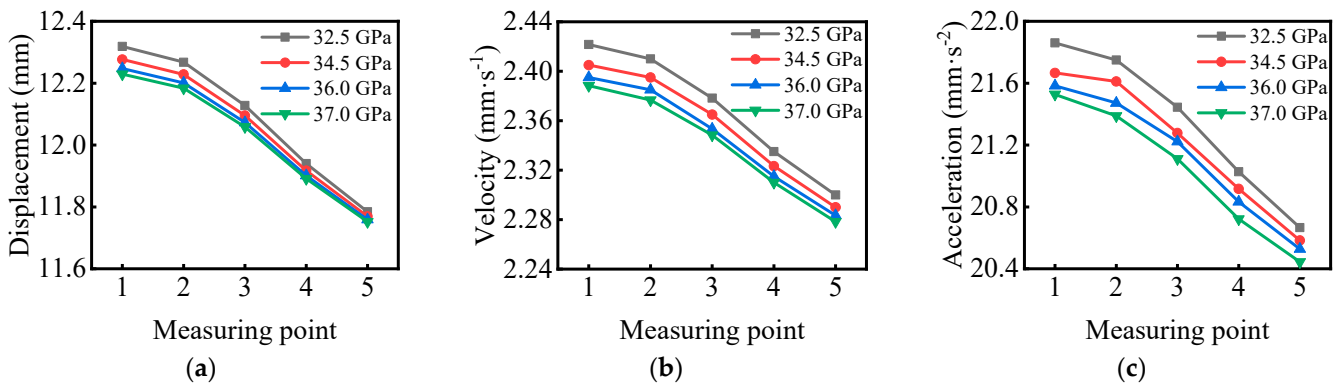


Figure 15. Peak value variation rule of different measuring points when the elastic modulus of concrete changes (a) displacement, (b) velocity, and (c) acceleration.

Table 3. Results of peak displacement, velocity, and acceleration at the mid–span measuring point when the elastic modulus of concrete changes.

Elastic Modulus of Concrete (GPa)	Displacement (mm)	Velocity (mm·s ⁻¹)	Acceleration (mm·s ⁻²)
32.5	12.3189	2.4217	21.8611
34.5	12.2768	2.405	21.6667
36.0	12.2477	2.3950	21.5833
37.0	12.2293	2.3883	21.5278

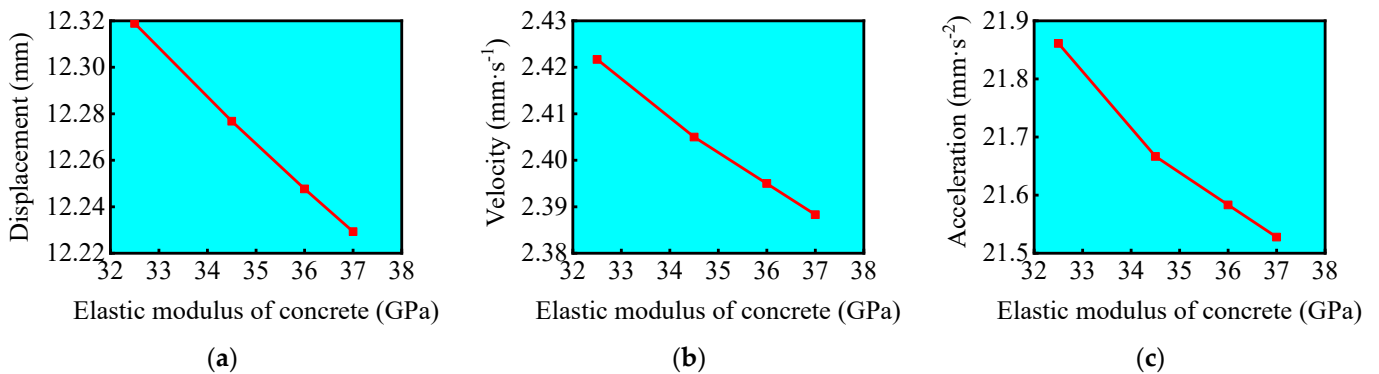


Figure 16. The law of mid–span peak value changing with elastic modulus of concrete (a) displacement, (b) velocity, and (c) acceleration.

5.2. Thickness of Overburden Layer

When the thickness of overburden layer changes, the displacement, velocity, and acceleration change rules of different measuring points of civil air defense construction caused by vehicle vibration change, as shown in Figure 17. The results of displacement, velocity, and acceleration peak values of mid–span measuring points are shown in Table 4. The displacement, velocity, and acceleration peak value change rules of mid–span measuring points are shown in Figure 18. When the overburden layer is 3, 4, 5, and 6 m thick, the peak displacement of the roof mid–span of the civil air defense construction is 12.3189, 11.3611, 10.1895, 8.7635 mm, respectively, the peak velocity is 2.4217, 2.1867, 1.9557, and 1.6773 mm·s⁻¹, respectively, and the peak acceleration is 21.8611, 18.4167, 16.275, 13.9222 mm·s⁻², respectively. The results show that the peak values of roof mid–span displacement, velocity, and acceleration decrease with the increase in the thickness of overburden layer. With the increase in the thickness of overburden layer by 33.33%, 66.67%, and 100%, the corresponding peak value of roof mid–span displacement decreases by 7.78%, 17.29%, and 28.86%, respectively, the peak value of velocity decreases by 9.70%, 19.24%, and 30.74%, respectively, and the peak value of acceleration decreases by 15.76%, 25.55%, and 36.32%, respectively.

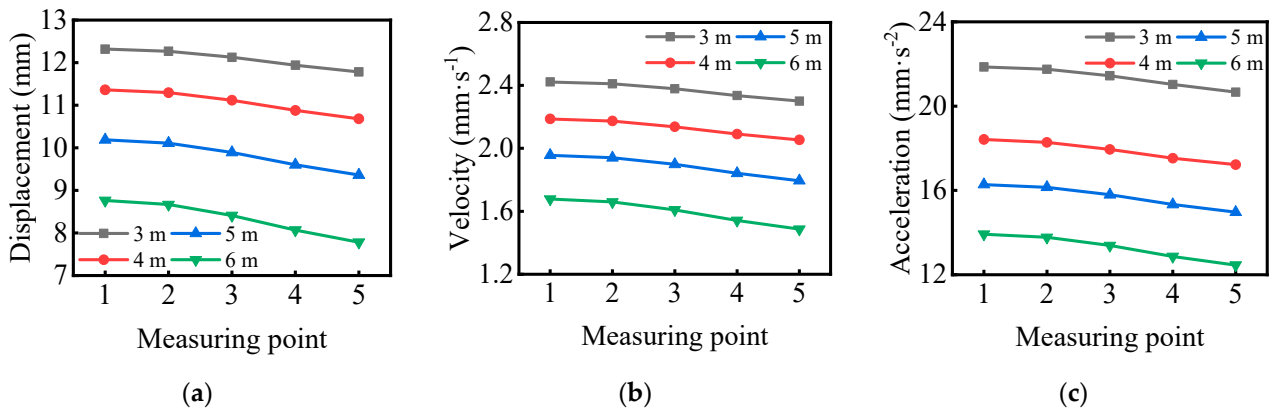


Figure 17. Peak value variation rule of different measuring points when the thickness of overburden layer changes (a) displacement, (b) velocity, and (c) acceleration.

Table 4. Results of peak displacement, velocity, and acceleration at the mid-span measuring point when the thickness of overburden layer changes.

Thickness of Overburden Layer (m)	Displacement (mm)	Velocity (mm·s ⁻¹)	Acceleration (mm·s ⁻²)
3	12.3189	2.4217	21.8611
4	11.3611	2.1867	18.4167
5	10.1895	1.9557	16.275
6	8.7635	1.6773	13.9222

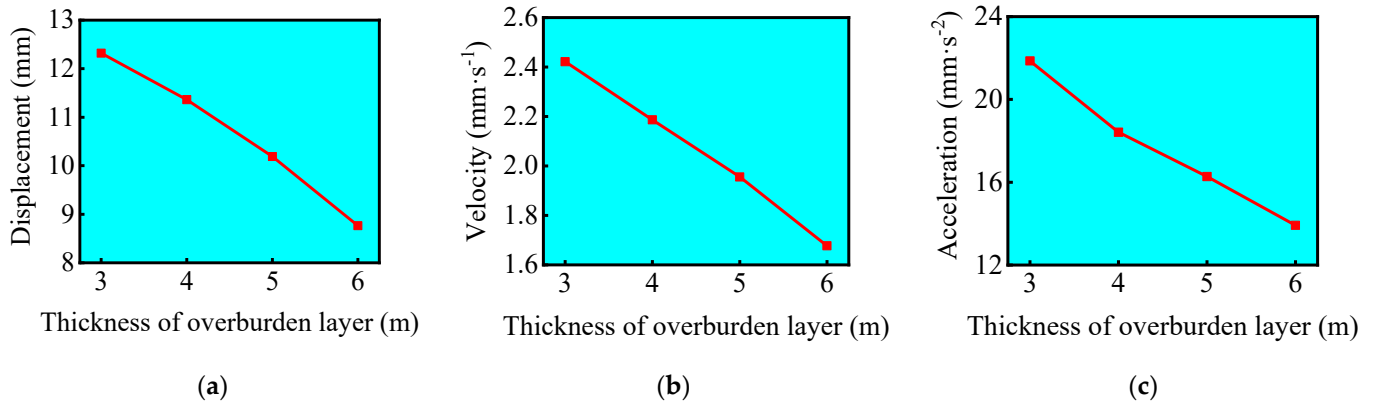


Figure 18. The law of mid-span peak value changing with thickness of overburden layer (a) displacement, (b) velocity, and (c) acceleration.

5.3. Density of Soil Layer

When the density of soil layer changes, the change rules of displacement, velocity, and acceleration at different measuring points of civil air defense construction caused by vehicle vibration are shown in Figure 19. The results of displacement, velocity, and acceleration peak values at mid-span measuring points are shown in Table 5. The change rules of displacement, velocity, and acceleration peak values at mid-span measuring points are shown in Figure 20. When the density of soil layer is 1750, 1800, 1850, and 1900 kg·m⁻³, the peak value of roof mid-span displacement of civil air defense construction is 26.623, 27.3133, 28.0004, and 28.6927 mm, respectively, the peak value of velocity is 5.1417, 5.2883, 5.4267, and 5.57 mm·s⁻¹, respectively, and the peak value of acceleration is 31.1389, 31.9167, 32.5278, and 33 mm·s⁻², respectively. The results show that the peak values of roof mid-span displacement, velocity, and acceleration increase with the increase in the density of soil layer. With the increase in the density of soil layer by 2.86%, 5.71%, and 8.57%, the corresponding peak value of roof mid-span displacement increases by 2.59%, 5.17%, and 7.77%, respectively, the peak value of velocity increases by 2.85%, 5.54%,

and 8.33%, respectively, and the peak value of acceleration increases by 2.50%, 4.46%, and 5.98%, respectively.

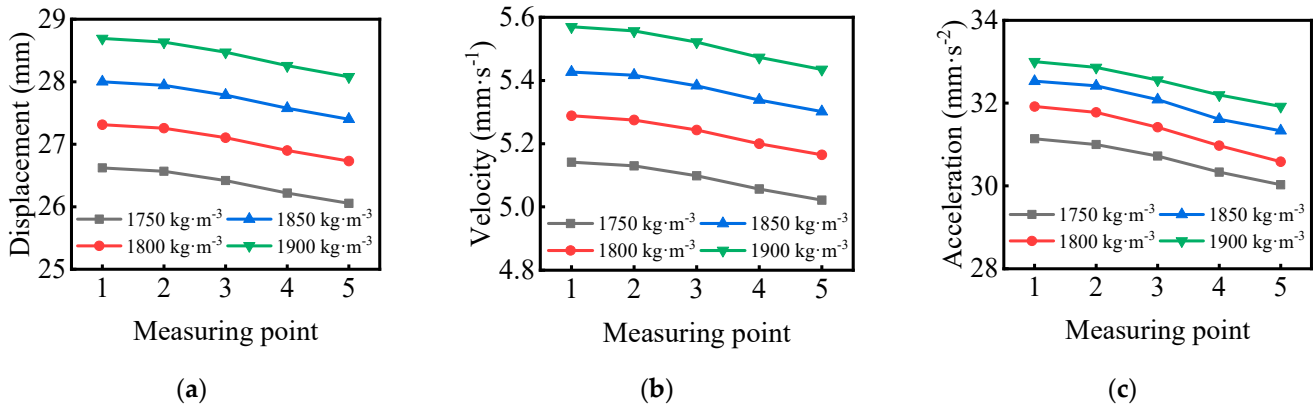


Figure 19. Peak value variation rule of different measuring points when the density of soil layer changes (a) displacement, (b) velocity, and (c) acceleration.

Table 5. Results of peak displacement, velocity, and acceleration at the mid–span measuring point when the density of soil layer changes.

Density of Soil Layer (kg·m ⁻³)	Displacement (mm)	Velocity (mm·s ⁻¹)	Acceleration (mm·s ⁻²)
1750	26.623	5.1417	31.1389
1800	27.3133	5.2883	31.9167
1850	28.0004	5.4267	32.5278
1900	28.6927	5.57	33

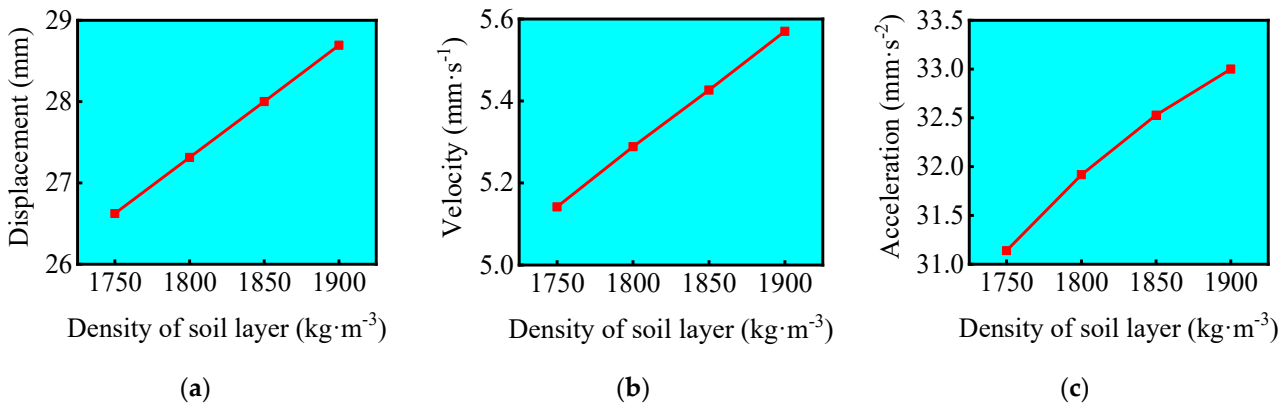


Figure 20. The law of mid–span peak value changing with density of soil layer (a) displacement, (b) velocity, and (c) acceleration.

5.4. Elastic Modulus of Soil Layer

When the elastic modulus of soil layer changes, the change rules of displacement, velocity, and acceleration at different measuring points of civil air defense construction caused by vehicle vibration are shown in Figure 21. The results of displacement, velocity, and acceleration peak values at mid–span measuring points are shown in Table 6. The change rules of displacement, velocity, and acceleration peak values at mid–span measuring points are shown in Figure 22. When the elastic modulus of soil layer is 1, 3, 5, and 7 MPa, the peak value of mid–span displacement of the roof of civil air defense construction is 81.4519, 27.3133, 16.625, and 12.0389 mm, the peak value of velocity is 15.4133, 5.2883, 3.27, and 2.37 mm·s⁻¹, and the peak value of acceleration is 56.3889, 18.25, 16.6667, and 16.6667 mm·s⁻². The results show that the peak values of displacement, velocity, and acceleration of roof mid–span decrease with the increase in elastic modulus

of soil layer. With the increase in elastic modulus of soil layer by 200%, 400%, and 600%, the corresponding peak values of roof mid–span displacement decrease by 66.47%, 79.59%, and 85.22%, respectively, the peak values of velocity decrease by 65.69%, 78.78%, and 84.62%, respectively, and the peak values of acceleration decrease by 43.40%, 54.83%, and 61.03%, respectively.

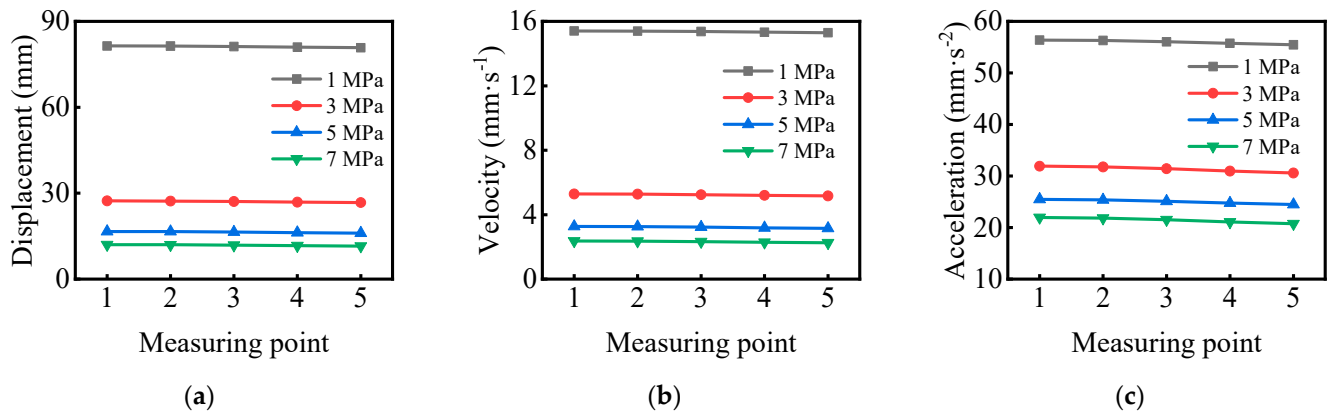


Figure 21. Peak value variation rule of different measuring points when the elastic modulus of soil layer changes (a) displacement, (b) velocity, and (c) acceleration.

Table 6. Results of peak displacement, velocity, and acceleration at the mid–span measuring point when the elastic modulus of soil layer changes.

Elastic Modulus of Soil Layer (MPa)	Displacement (mm)	Velocity (mm·s ⁻¹)	Acceleration (mm·s ⁻²)
1	81.4519	15.4133	56.3889
3	27.3133	5.2883	31.9167
5	16.625	3.27	25.4722
7	12.0389	2.37	21.9722

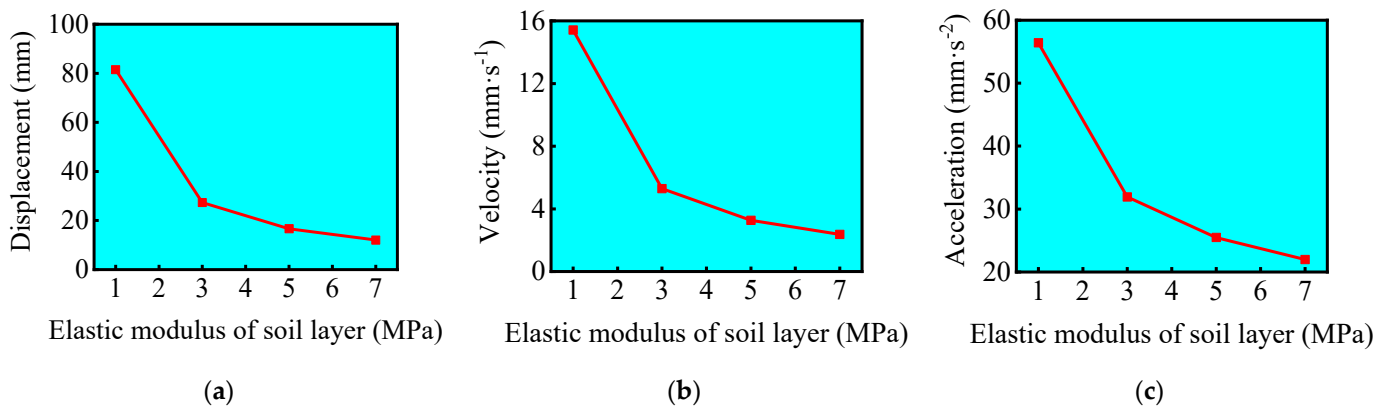


Figure 22. The law of mid–span peak value changing with elastic modulus of soil layer (a) displacement, (b) velocity, and (c) acceleration.

5.5. Vehicle Speed

When the vehicle speed changes, the change rules of displacement, velocity, and acceleration at different measuring points of civil air defense construction caused by vehicle vibration are shown in Figure 23. The results of displacement, velocity, and acceleration peak values at mid–span measuring points are shown in Table 7. The change rules of displacement, velocity, and acceleration peak values at mid–span measuring points are shown in Figure 24. When the vehicle speed is 15, 30, 45, and 60 km/h, the peak value of the mid–span displacement of the roof of the civil air defense construction is 12.2992, 12.3147, 12.3165, and 12.3189 mm, respectively, the peak value of the speed is 1.8479, 2.2667, 2.3813,

and $2.4217 \text{ mm}\cdot\text{s}^{-1}$, respectively, and the peak value of the acceleration is 12.1545, 19.1111, 20.8906, and $21.8611 \text{ mm}\cdot\text{s}^{-2}$, respectively. The results show that the roof mid-span displacement, velocity, and acceleration peak values increase with the increase in vehicle speed. With the increase in vehicle speed by 100%, 200%, and 300%, the corresponding roof mid-span displacement peak values increase by 0.13%, 0.14%, and 0.16%, respectively, the velocity peak values decrease by 22.66%, 28.86%, and 31.05%, respectively, and the acceleration peak values decrease by 57.23%, 71.88%, and 79.86%, respectively.

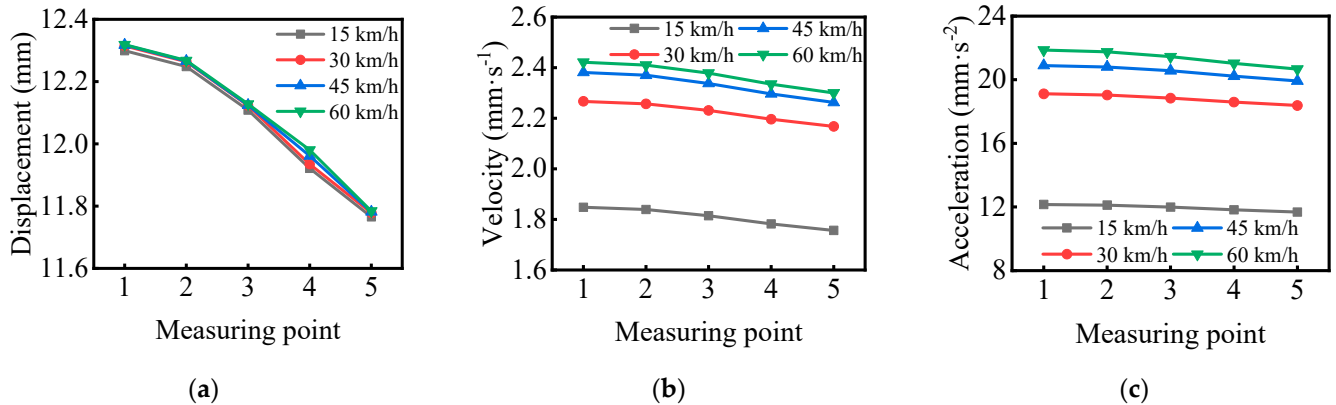


Figure 23. Peak value variation rule of different measuring points when the vehicle speed changes (a) displacement, (b) velocity, and (c) acceleration.

Table 7. Results of peak displacement, velocity, and acceleration at the mid-span measuring point when the vehicle speed changes.

Vehicle Speed (km/h)	Displacement (mm)	Velocity ($\text{mm}\cdot\text{s}^{-1}$)	Acceleration ($\text{mm}\cdot\text{s}^{-2}$)
15	12.2992	1.8479	12.1545
30	12.3147	2.2667	19.1111
45	12.3165	2.3813	20.8906
60	12.3189	2.4217	21.8611

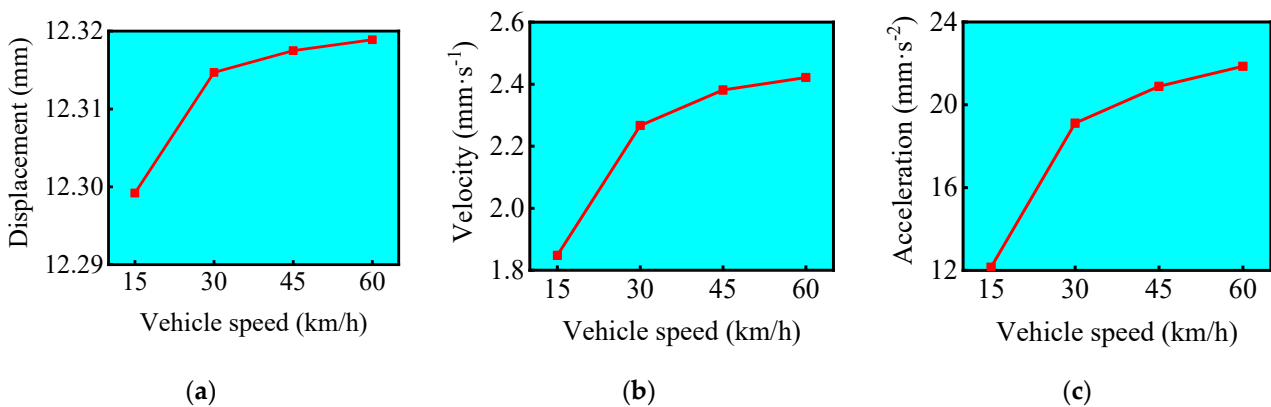


Figure 24. The law of mid-span peak value changing with vehicle speed (a) displacement, (b) velocity, and (c) acceleration.

5.6. Vehicle Mass

When the vehicle mass changes, the change rules of displacement, velocity, and acceleration at different measuring points of civil air defense construction caused by vehicle vibration are shown in Figure 25. The results of displacement, velocity, and acceleration peak values at mid-span measuring points are shown in Table 8. The change rules of displacement, velocity, and acceleration peak values at mid-span measuring points are shown in Figure 26. When the vehicle mass is 20, 40, 60, and 80 kN, the peak value of the

mid-span displacement of the roof of the civil air defense construction is 12.3189, 12.3193, 12.3251, and 12.3336 mm, respectively, the peak value of the velocity is 2.4217, 2.4283, 2.4395, and 2.4505 mm·s⁻¹, respectively, and the peak value of the acceleration is 21.8611, 21.9722, 22.1111, and 22.2778 mm·s⁻², respectively. The results show that the peak value of roof mid-span displacement and acceleration increases with the increase in vehicle mass. With the increase in vehicle mass by 100%, 200%, and 300%, the corresponding peak value of roof mid-span displacement increases by 0.003%, 0.05%, and 0.12%, respectively, the peak value of speed decreases by 0.28%, 0.74%, and 1.19%, respectively, and the peak value of acceleration increases by 0.51%, 1.14%, and 1.91%, respectively.

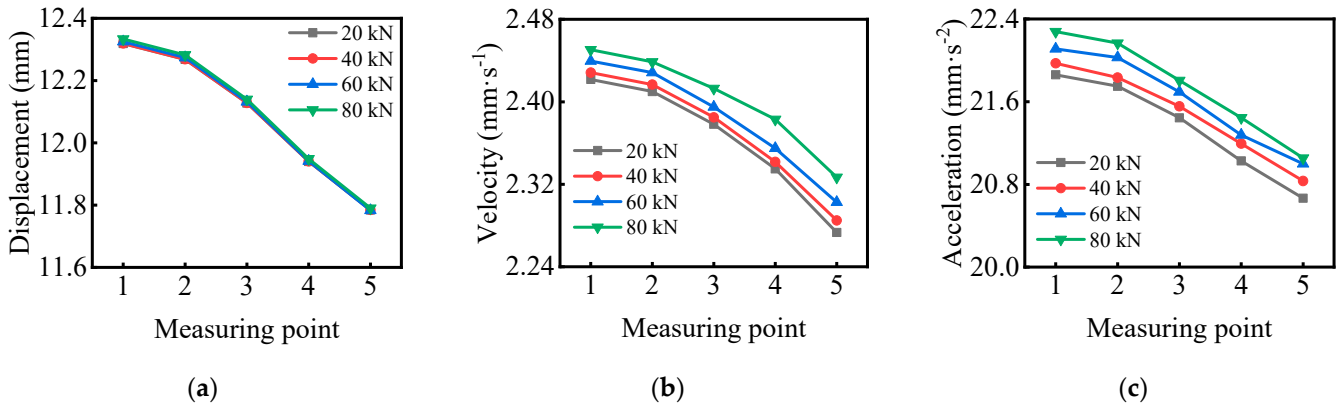


Figure 25. Peak value variation rule of different measuring points when the vehicle mass changes (a) displacement, (b) velocity, and (c) acceleration.

Table 8. Results of peak displacement, velocity, and acceleration at the mid-span measuring point when the vehicle mass changes.

Vehicle Mass (kN)	Displacement (mm)	Velocity (mm·s ⁻¹)	Acceleration (mm·s ⁻²)
20	12.3189	2.4217	21.8611
40	12.3193	2.4283	21.9722
60	12.3251	2.4395	22.1111
80	12.3336	2.4505	22.2778

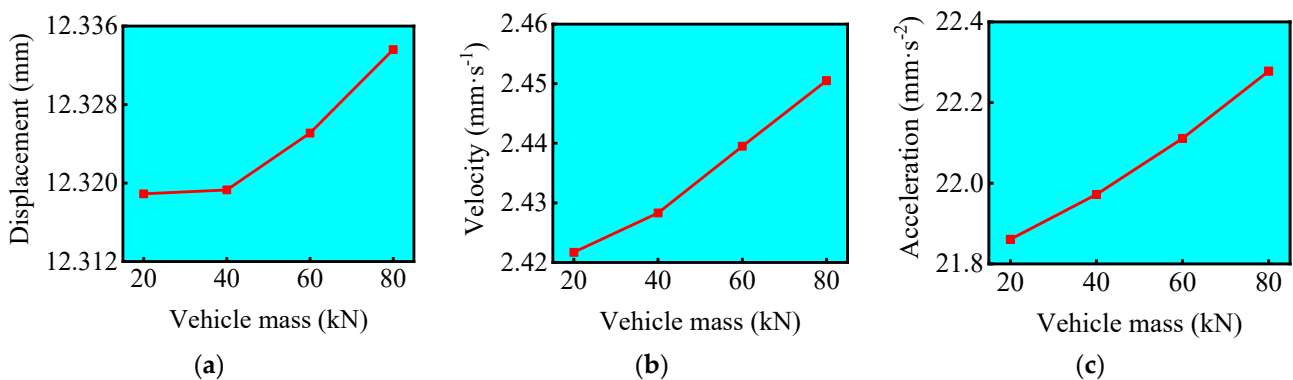


Figure 26. The law of mid-span peak value changing with vehicle mass (a) displacement, (b) velocity, and (c) acceleration.

6. Sensitivity Analysis of Influencing Factors

According to the above simulation results, the change value of each influence parameter is selected as the comparison matrix X , and the displacement Y_a , velocity Y_b , and acceleration Y_c under the corresponding conditions are taken as the reference matrix. The comparison matrix and reference matrix are established, and the grey correlation degree of

the influencing factors of civil air defense construction vibration caused by vehicle vibration is calculated.

$$X = \begin{pmatrix} X_1 \\ X_2 \\ X_3 \\ X_4 \\ X_5 \\ X_6 \end{pmatrix} = \begin{pmatrix} 32.5 & 34.5 & 36.0 & 37.0 \\ 3 & 4 & 5 & 6 \\ 1750 & 1800 & 1850 & 1900 \\ 1 & 3 & 5 & 7 \\ 15 & 30 & 45 & 60 \\ 20 & 40 & 60 & 80 \end{pmatrix} \tag{15}$$

$$Y_a = \begin{pmatrix} Y_{a1} \\ Y_{a2} \\ Y_{a3} \\ Y_{a4} \\ Y_{a5} \\ Y_{a6} \end{pmatrix} = \begin{pmatrix} 12.3189 & 12.2768 & 12.2477 & 12.2293 \\ 12.3189 & 11.3611 & 10.1895 & 8.7635 \\ 26.6230 & 27.3133 & 28.0004 & 28.6927 \\ 81.4519 & 27.3133 & 16.6250 & 12.0389 \\ 12.2992 & 12.3147 & 12.3175 & 12.3189 \\ 12.3189 & 12.3193 & 12.3251 & 12.3336 \end{pmatrix} \tag{16}$$

$$Y_b = \begin{pmatrix} Y_{b1} \\ Y_{b2} \\ Y_{b3} \\ Y_{b4} \\ Y_{b5} \\ Y_{b6} \end{pmatrix} = \begin{pmatrix} 2.4217 & 2.405 & 2.395 & 2.3883 \\ 2.4217 & 2.1867 & 1.9557 & 1.6773 \\ 5.1417 & 5.2883 & 5.4267 & 5.57 \\ 15.4133 & 5.2883 & 3.27 & 2.37 \\ 1.8479 & 2.2667 & 2.3813 & 2.4217 \\ 2.4217 & 2.4283 & 2.4395 & 2.4505 \end{pmatrix} \tag{17}$$

$$Y_c = \begin{pmatrix} Y_{c1} \\ Y_{c2} \\ Y_{c3} \\ Y_{c4} \\ Y_{c5} \\ Y_{c6} \end{pmatrix} = \begin{pmatrix} 21.8611 & 21.6667 & 21.5833 & 21.5278 \\ 21.8611 & 18.4167 & 16.275 & 13.9222 \\ 31.1389 & 31.9167 & 32.5278 & 33 \\ 56.3889 & 31.9167 & 25.4722 & 21.9722 \\ 12.1545 & 19.1111 & 20.8906 & 21.8611 \\ 21.8611 & 21.9722 & 22.1111 & 22.2778 \end{pmatrix} \tag{18}$$

According to Equations (5) and (6):

$$X' = \begin{pmatrix} 0 & 0.4444 & 0.7778 & 1 \\ 0 & 0.3333 & 0.6667 & 1 \\ 0 & 0.3333 & 0.6667 & 1 \\ 0 & 0.3333 & 0.6667 & 1 \\ 0 & 0.3333 & 0.6667 & 1 \\ 0 & 0.3333 & 0.6667 & 1 \end{pmatrix} \tag{19}$$

$$Y'_a = \begin{pmatrix} 1 & 0.5301 & 0.2054 & 0 \\ 1 & 0.7306 & 0.4011 & 0 \\ 0 & 0.3335 & 0.6655 & 1 \\ 1 & 0.2201 & 0.0661 & 0 \\ 0 & 0.7868 & 0.9289 & 1 \\ 0 & 0.0272 & 0.4218 & 1 \end{pmatrix} \tag{20}$$

$$Y'_b = \begin{pmatrix} 1 & 0.5 & 0.2001 & 0 \\ 1 & 0.6843 & 0.3739 & 0 \\ 0 & 0.3424 & 0.6654 & 1 \\ 1 & 0.2237 & 0.0690 & 0 \\ 0 & 0.7298 & 0.9296 & 1 \\ 0 & 0.2310 & 0.6185 & 1 \end{pmatrix} \tag{21}$$

$$Y'_b = \begin{pmatrix} 1 & 0.5 & 0.2001 & 0 \\ 1 & 0.6843 & 0.3739 & 0 \\ 0 & 0.3424 & 0.6654 & 1 \\ 1 & 0.2237 & 0.0690 & 0 \\ 0 & 0.7298 & 0.9296 & 1 \\ 0 & 0.2310 & 0.6185 & 1 \end{pmatrix} \tag{22}$$

The discernibility matrix is obtained from Equation (7):

$$\Delta_a = \begin{pmatrix} 1 & 0.0857 & 0.5724 & 1 \\ 1 & 0.3973 & 0.2656 & 1 \\ 0 & 0.0002 & 0.0012 & 0 \\ 1 & 0.1132 & 0.6006 & 1 \\ 0 & 0.4535 & 0.2622 & 0 \\ 0 & 0.3061 & 0.2449 & 0 \end{pmatrix} \tag{23}$$

$$\Delta_b = \begin{pmatrix} 1 & 0.0556 & 0.5777 & 1 \\ 1 & 0.3510 & 0.2928 & 1 \\ 0 & 0.0091 & 0.0013 & 0 \\ 1 & 0.1096 & 0.5977 & 1 \\ 0 & 0.3965 & 0.2629 & 0 \\ 0 & 0.1023 & 0.0482 & 0 \end{pmatrix} \tag{24}$$

$$\Delta_c = \begin{pmatrix} 1 & 0.0277 & 0.6111 & 1 \\ 1 & 0.2328 & 0.3703 & 1 \\ 0 & 0.0846 & 0.0796 & 0 \\ 1 & 0.0444 & 0.5650 & 1 \\ 0 & 0.3834 & 0.2333 & 0 \\ 0 & 0.0666 & 0.0667 & 0 \end{pmatrix} \tag{25}$$

where $\Delta_{max} = \max(\Delta_{ij})$; $\Delta_{min} = \min(\Delta_{ij})$, the resolution coefficient is generally taken $\xi = 0.5$.

The grey correlation coefficient matrix is obtained from Equation (9):

$$\gamma_a = \begin{pmatrix} 0.3333 & 0.8537 & 0.4662 & 0.3333 \\ 0.3333 & 0.5572 & 0.6531 & 0.3333 \\ 1 & 0.9996 & 0.9976 & 1 \\ 0.3333 & 0.8154 & 0.4543 & 0.3333 \\ 1 & 0.5244 & 0.6560 & 1 \\ 1 & 0.6203 & 0.6712 & 1 \end{pmatrix} \tag{26}$$

$$\gamma_b = \begin{pmatrix} 0.3333 & 0.8999 & 0.4640 & 0.3333 \\ 0.3333 & 0.5875 & 0.6307 & 0.3333 \\ 1 & 0.9821 & 0.9974 & 1 \\ 0.3333 & 0.8202 & 0.4555 & 0.3333 \\ 1 & 0.5577 & 0.6554 & 1 \\ 1 & 0.8302 & 0.9121 & 1 \end{pmatrix} \tag{27}$$

$$\gamma_c = \begin{pmatrix} 0.3333 & 0.9475 & 0.4500 & 0.3333 \\ 0.3333 & 0.6823 & 0.5745 & 0.3333 \\ 1 & 0.8553 & 0.8627 & 1 \\ 0.3333 & 0.9184 & 0.4695 & 0.3333 \\ 1 & 0.5660 & 0.6818 & 1 \\ 1 & 0.8825 & 0.8823 & 1 \end{pmatrix} \tag{28}$$

Then according to Equation (10), the grey correlation degree sequence is:

$$A_a = (0.4966, 0.4692, 0.9993, 0.4841, 0.7951, 0.8229)^T \tag{29}$$

$$A_b = (0.5076, 0.4712, 0.9949, 0.4856, 0.8033, 0.9356)^T \quad (30)$$

$$A_c = (0.5160, 0.4809, 0.9295, 0.5136, 0.8120, 0.9412)^T \quad (31)$$

The grey correlation degree of the influencing factors of displacement and velocity is obtained as follows: density of soil layer > vehicle mass > vehicle speed > elastic modulus of concrete > elastic modulus of soil layer > thickness of overburden layer. The order of grey correlation degree of the influencing factors of acceleration is: vehicle mass > density of soil layer > vehicle speed > elastic modulus of concrete > elastic modulus of soil layer > thickness of overburden layer. The density of soil layer, vehicle mass, and vehicle speed have a great impact on the displacement, velocity, and acceleration of civil air defense construction, and their grey correlation degrees are 0.7951–0.9993, 0.8033–0.9949, and 0.8120–0.9295, respectively. For projects with low soil density, the seismic performance of underground constructions should be strengthened during design. For roads with different traffic levels, the underground construction should be designed and constructed differently. For example, when the traffic speed and load capacity of the road are strong, the seismic performance of the underground constructions should be strengthened.

When the six influencing factors change, the displacement, velocity, and acceleration at the mid–span position of the roof are all the maximum, which indicates that it is the most dangerous and requires key monitoring and protection. In case of a large span, temporary support can be added in the middle of the span during design and construction.

7. Conclusions

This paper is based on the civil air defense project at the intersection of Zhongzhou Middle Road and Shachang South Road in Luoyang City. In order to study the influence of various factors on civil air defense construction vibration under vehicle load, first refer to the actual project on site, then use ANSYS to conduct numerical simulation calculation, and finally use the grey correlation method to conduct sensitivity analysis on the elastic modulus of concrete, thickness of overburden layer, density of soil layer, elastic modulus of soil layer, vehicle speed, and vehicle mass. The following conclusions are obtained:

1. The displacement, velocity, and acceleration at the mid–span position of the civil air defense roof are the largest, and they are smaller and smaller along the roof from the mid–span position to the wall;
2. It can be seen from the field monitoring that when the vibration acceleration is less than $\pm 100 \text{ mm}\cdot\text{s}^{-2}$, the impact of vehicle traffic on the excavation is small, but when the acceleration is more than $\pm 100 \text{ mm}\cdot\text{s}^{-2}$, the impact is obvious, and there are adverse effects such as sand loss;
3. The grey correlation degree of the influencing factors of displacement and velocity is density of soil layer, vehicle mass, vehicle speed, elastic modulus of concrete, elastic modulus of soil layer, and thickness of overburden layer from large to small. The grey correlation degree of the influencing factors of acceleration from large to small is the vehicle mass, density of soil layer, vehicle speed, elastic modulus of concrete, elastic modulus of soil layer, and thickness of overburden layer;
4. The density of soil layer, vehicle mass, and vehicle speed have a great impact on the displacement, speed, and acceleration of civil air defense construction, with the grey correlation degree of 0.7951–0.9993.

Author Contributions: Conceptualization, H.Z. (Hui Zhou); methodology, Y.W.; software, Y.W.; validation, Y.W. and C.M.; formal analysis, Y.W.; investigation, H.Z. (Hui Zhang); resources, C.M.; data curation, Y.W.; writing—original draft preparation, Y.W.; writing—review and editing, Y.W.; visualization, Y.W.; supervision, C.M.; project administration, C.M.; funding acquisition, C.M. All authors have read and agreed to the published version of the manuscript.

Funding: This research was funded by the Postgraduate Scientific Research Project for Anhui Universities (YJS20210393).

Institutional Review Board Statement: Not applicable.

Informed Consent Statement: Not applicable.

Data Availability Statement: The data used to support the findings of this study are available from the corresponding author upon request.

Conflicts of Interest: The authors declare no conflict of interest.

References

1. Qian, Q. Present state, problems and development trends of urban underground space in China. *Undergr. Space Technol.* **2016**, *55*, 280–289.
2. Zhao, J.; Kunzli, O. An introduction to connectivity concept and an example of physical connectivity evaluation for underground space. *Undergr. Space Technol.* **2016**, *55*, 205–213. [[CrossRef](#)]
3. Chen, Z.; Chen, J.; Liu, H.; Zhang, Z. Present status and development trends of underground space in Chinese cities: Evaluation and analysis. *Undergr. Space Technol.* **2018**, *71*, 253–270. [[CrossRef](#)]
4. Wu, Y.; Mu, C.; Zong, Q.; Wu, J.; Zhou, H. Study on blasting vibration control of brick-concrete structure under subway tunnel. *Appl. Sci.* **2022**, *12*, 10960. [[CrossRef](#)]
5. Wu, J.; Zhao, J.; Tan, Z.; Liu, X.; Wang, X.; Liu, M. Mechanical behavior of large-diameter adjacent shield tunnelling bridge piles: A case study of Chunfeng tunnel. *Appl. Sci.* **2022**, *12*, 5418. [[CrossRef](#)]
6. Qiu, C.; Zheng, Y.; Zhang, Y.; Tan, W.; Zhao, S. Discussion on classification method and criterion for the deep-buried and shallow-buried rock tunnels. *Mod. Tunn. Technol.* **2019**, *56*, 14–21.
7. Yao, Y.; Fang, Y.; Li, S.; Zhuo, B. Analysis of mechanical behavior of lining structure of high-filled cut-and-cover tunnel based on DEM. *Arab. J. Sci. Eng.* **2022**, *47*, 12729–12743. [[CrossRef](#)]
8. Li, S.; Zhao, L.; Ho, I.; Ning, G.; Yu, B.; Wang, C. Influence of structural shape on earth pressure for high-filled cut-and-cover tunnel with and without load reduction based on discrete element method. *Adv. Civ. Eng.* **2020**, *2020*, 8877873. [[CrossRef](#)]
9. Li, S.; Jianie, Y.; Ho, I.; Ma, L.; Yu, B.; Wang, C. Evolution of load reduction for high-filled cut-and-cover tunnels subjected to soil creep. *Int. J. Geomech.* **2021**, *21*, 04021172. [[CrossRef](#)]
10. Ptilakis, K.; Tsinidis, G. Performance and seismic design of underground structures. In *Earthquake Geotechnical Engineering Design*, 1st ed.; Maugeri, M., Soccodato, C., Eds.; Springer International Publishing: Cham, Switzerland, 2014; Volume 28, pp. 279–340. [[CrossRef](#)]
11. Cardone, D.; Viggiani, L.; Perrone, G.; Telesca, A.; Di Cesare, A.; Ponzio, F.; Ragni, L.; Micozzi, F.; Dall’Asta, A.; Furinghetti, M.; et al. Modelling and Seismic Response Analysis of Existing Italian Residential RC Buildings Retrofitted by Seismic Isolation. *J. Earthq. Eng.* **2022**. early access. [[CrossRef](#)]
12. Zou, B.; Wang, J.; Tian, Q.; Guo, W.; Yang, J.; Yi, J.; Lou, Z. Numerical analysis of the soil deformation caused by tunneling under vehicle loads in the coastal reclamation area. *Math. Probl. Eng.* **2015**, *2015*, 937245. [[CrossRef](#)]
13. Zhang, Z.; Zhang, X.; Cui, Y.; Qiu, H. Discrete element modeling of a cross-river tunnel under subway train operation during peak and off-peak periods. *Arab. J. Geosci.* **2019**, *12*, 102. [[CrossRef](#)]
14. Li, C.; Zhang, W.; Wang, X.; Pan, B.; Zhu, H.; Spencer, B. Modeling dynamic responses of a cross-river road shield tunnel under stochastic vehicle loads. *Tunn. Undergr. Space Technol.* **2020**, *102*, 103432. [[CrossRef](#)]
15. Li, C.; Jiang, S.; Li, J.; Huang, J. Bayesian approach for sequential probabilistic back analysis of uncertain geomechanical parameters and reliability updating of tunneling-induced ground settlements. *Adv. Civ. Eng.* **2020**, *2020*, 8528304. [[CrossRef](#)]
16. Zhou, J.; Chen, Y.; Kuang, Y.; Xu, J. Dynamic response and long-term accumulation deformation of saturated soft clay under repeated load of subway trains. *Sci. Technol. Eng.* **2018**, *18*, 137–143.
17. Wang, H.; Markine, V. Modelling of the long-term behaviour of transition zones: Prediction of track settlement. *Eng. Struct.* **2018**, *156*, 294–304. [[CrossRef](#)]
18. Meng, S.; Zhou, J.; Wang, M.; Cheng, Y.; Sun, Y. Analysis on the deformation characteristics for roadbed under vehicle loads. *Earthq. Eng. Eng. Dynam.* **2018**, *38*, 35–41.
19. Shi, L.; He, J.; Huang, Z.; Sun, H.; Yuan, Z. Numerical investigations on influences of tunnel differential settlement on saturated poroelastic ground vibrations and lining forces induced by metro train. *Soil Dynam. Earthq. Eng.* **2022**, *156*, 107202. [[CrossRef](#)]
20. Ma, L.; Zhang, J.; Liu, Y. Study on the dynamic characteristics of remolded loess in Shanxi expressway subgrade under vehicle loads. *China Earthq. Eng. J.* **2018**, *40*, 101–104.
21. Shao, Z.; Fan, Y.; Wang, X. Research into the effect of traffic load on stability of shallow buried loess tunnel. *Chin. J. Appl. Mech.* **2016**, *33*, 299–305.
22. Jia, Y.; Liu, W.; Sun, X.; Liu, W.; Zhang, H. Vibration effect on surroundings induced by passing trains in spatial overlapping tunnels. *J. China Railw. Soc.* **2009**, *31*, 104–109.
23. Galvin, P.; Dominguez, J. High-speed train-induced ground motion and interaction with structures. *J. Sound Vib.* **2007**, *307*, 755–777. [[CrossRef](#)]
24. Zhou, S.; Zhang, X.; Di, H.; He, C. Metro train-track-tunnel-soil vertical dynamic interactions—semi-analytical approach. *Veh. Syst. Dyn.* **2018**, *56*, 1945–1968. [[CrossRef](#)]

25. Hu, J.; Bian, X. Experimental and numerical studies on dynamic responses of tunnel and soils due to train traffic loads. *Tunn. Undergr. Space Technol.* **2022**, *128*, 104628. [[CrossRef](#)]
26. Yan, Q.; Chen, H.; Chen, W.; Zhang, J.; Ma, S.; Huang, X. Dynamic Characteristic and fatigue accumulative damage of a cross shield tunnel structure under vibration load. *Shock Vib.* **2018**, *2018*, 9525680. [[CrossRef](#)]
27. Yang, W.; Deng, E.; Shi, C.; Liu, N.; Fei, R.; Yue, H. Lining fatigue test and influence zoning of tridimensional cross-tunnel under high-speed train loads. *Appl. Sci.* **2020**, *10*, 5694. [[CrossRef](#)]
28. Zhang, Z.; Zeng, B.; Da, C.; He, W. Study on structural service performance of heavy-haul railway tunnel with voided base. *Adv. Civ. Eng.* **2018**, *2018*, 3510979. [[CrossRef](#)]
29. Lai, J.; Wang, K.; Qiu, J.; Niu, F.; Wang, J.; Chen, J. Vibration response characteristics of the cross tunnel structure. *Shock Vib.* **2016**, *2016*, 9524206. [[CrossRef](#)]
30. Deng, J. *Grey Theory*, 1st ed.; Huazhong University of Science and Technology Press: Wuhan, China, 2002; pp. 1–15.
31. Liu, S.; Guo, T.; Dang, Y. *Grey System Theory and Its Application*, 2nd ed.; Science Press: Beijing, China, 1999; pp. 1–20.
32. Hu, W.; Zhao, Q.; Liu, Y.; Li, Z.; Kong, X. Damage evaluation of the paving around manholes under vehicle dynamic load. *Adv. Mater. Sci. Eng.* **2020**, *2020*, 6510439. [[CrossRef](#)]
33. Xie, L.; Wu, C.; Duan, M.; Lyu, N. Analysis of freeway safety influencing factors on driving workload and performance based on the gray correlation method. *J. Adv. Transport.* **2021**, *2021*, 6566207. [[CrossRef](#)]
34. Liu, F.; He, F.; Wu, Y.; Li, H.; Gao, Y. Influence of vehicle vibration on construction of shallow buried excavation. *Sci. Technol. Eng.* **2021**, *21*, 9081–9087.
35. Liu, F.; Wang, H.; Li, H.; Huang, X. Numerical analysis on ultra-shallow buried excavation method in underground commercial street. *Chin. J. Undergr. Space Eng.* **2021**, *17*, 180–186.
36. Zhang, Y.; Liang, B. Dynamic response to subgrade of highway in geometric irregularity condition. *J. Lanzhou Railw. Univ. Nat. Sci.* **2001**, *20*, 66–69.